ORIGINAL ARTICLE

lajss.org© Latin American Journal of Solids and Structures

www.lajss.org

Ultimate Bending Strength Evaluation of MVFT Composite Girder by using Finite Element Method and Machine Learning Regressors

Zhihua Xiong [a]* , Jiawen Li [a] , Houda Zhu [a] , Xuyao Liu [a] , Zhuoxi Liang [a]

[a]Department of Civil Engineering, College of Water Resources and Architectural Engineering, Northwest A&F University, Yangling, China. Email: xiongzhihua_2013@126.com, ljwxncq-686@nwafu.edu.cn, zhuhd2020@nwafu.edu.cn, xy.liu@nwafu.edu.cn, 2017012333@nwafu.edu.cn

* Corresponding author

https://doi.org/10.1590/1679-78257006

Abstract

This paper has evaluated the bending performance of a novel prefabricated MVFT steel-concrete composite girder. 9 meters pilot MVFT girder was analyzed by validated finite element model. In the pilot test, the height of web, the length of grouted concrete in the girder and net spacing between webs were parametrically modeled to discuss their effect to the bending strength. An ultimate bending strength formula has been obtained, which was based on the regression of parametric results. In the meantime, the two Machine Learning (ML) models, BP neural network and Least Squares Support Vector Machine, have been also implemented to train and then predict the ultimate strength of MVFT girder. Three factors were selected as input in ML models: the distance between steel girder's Tensile Centroid(TC) and slab's Compressive Centroid(CC), the distance between steel girder's TC and its CC, the compressive area of steel girder. After the completion of the ML training, the ultimate strength predictions of 30 meters MVFT girder by BP model and the formula have been compared, which agrees well with each other and validates their accuracy.

Keywords

MVFT girder, ultimate bending strength, artificial neural networks, composite dowel, failure mode, LSSVM

Graphical Abstract

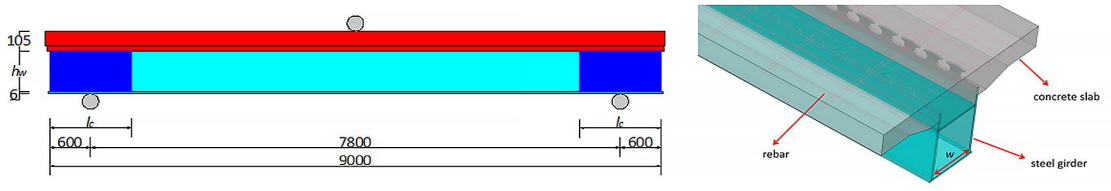

The overall and detailed finite element model of MVFT girder(unit:mm)

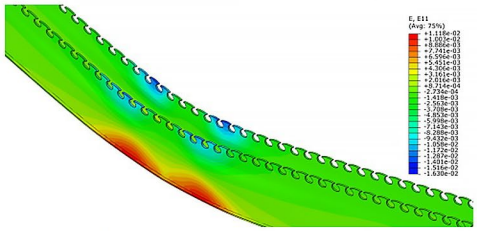

The tensile strain of the steel girder

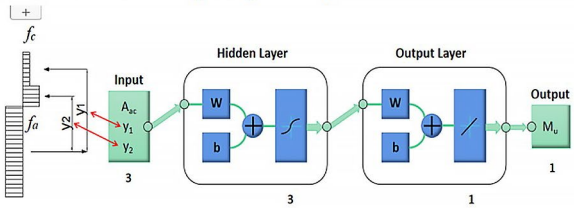

The flow chart of the BP neural network

Received February 18, 2022. In revised form March 08, 2022. Accepted March 08, 2022. Available online March 09, 2022.
https://doi.org/10.1590/1679-78257006

1 INTRODUCTION

Steel-concrete composite bridge has the merits of light weight and excellent fatigue performance in long-span bridges, therefore, they are widely employed in Bridge Engineering (Svensson, 2013; Liu et al., 2015). With respect to the small-span bridges, German scholars have reformed the shear connections of conventional steel-concrete composite girder and proposed VFT (Verbund- Fertigteil-Trager) composite girder, which has been used in Germany and other European countries since 1998 (Petzek and Bancila, 2010). Hechler et al. (2011) and Kołakowski and Lorenc (2015) introduced the construction technology and its engineering practices. Zanon et al. (2021) proposed the VFT-RS(Rolled Section) composite girder on the basis of VFT technology, which can further improve the structural efficiency and take full advantages of high strength of steel. The composite dowel as shear connector is the innovation of VFT girder, which is different from typical steel-concrete composite girder. Harnatkiewicz et al. (2011) and Berthellemy et al. (2018) studied the fatigue performance of composite dowel, and they suggested an optimized dowel's shape to improve its fatigue performance.

For the cold and high-altitude region, the authors proposed a small-span prefabricated MVFT steel-concrete composite girder, which is evolved from VFT girder. The steel girder and the concrete slab of MVFT girder are both prefabricated in the mill, without secondary casting (Xiong et al., 2018; Xiong, 2021; Chen et al., 2021). MVFT composite girder has the merits of convenient fabrication, light weight, fast construction and time-saving.

The ultimate bending capacity of steel-concrete composite girders is the focus of theoretical analysis and engineering design. Non-plastic and plastic analysis are the two typical methods to calculate the flexural capacity of the composite girder. Yang et al. (2018) proposed a formula for calculating the flexural capacity of composite girders in the sagging moment region by adopting the elastoplastic section analysis method and introducing the reduction coefficient of flexural capacity. Liang et al. (2005) studied the flexural and shear bearing capacity of simply supported composite girders under combined moment and shear; Liu et al. (2019) studied the flexural strength of steel-concrete simply supported composite girders under hogging bending moment. Ryu et al. (2006) studied the stiffness and strength of composite girders with Class 3 section under bending moment through 4-point flexural test. Zhang et al. (2020) studied the degradation process of flexural capacity of composite box girders under fire through numerical simulation. In this paper, the plastic method is adopted to calculate the ultimate bending capacity of MVFT girder due to its clear concept, concise form and extensive use.

In recent years, machine learning (ML) has developed rapidly and been applied to damage detection and fire resistance evaluation of composite girders. Abdeljaber et al. (2018) estimated the actual amount of vibration-based structural damage by using an enhanced CNN-based approach. Tan et al. (2020) used the normalized value of modal strain energy-based damage index Z as the input layer to locate and quantify the damage of composite girders, and the feasibility of this method through several numerical examples were verified. Hakim and Razak (2013) used the first five natural frequencies as the input layer to train neural networks, and then used them to predict the severity of damage. Tadesse et al. (2012) proposed three neural networks with the number of input layer parameters of 3, 7 and 8 respectively, to predict mid-span deflection of simply supported, two-span and three-span composite girder bridges. Li et al. (2021) used the neural network with 7 inputs, 3 outputs and 2 hidden layers to predict the fire resistance of concrete encased steel (CES) composite columns with concrete grade up to C120. In addition, machine learning has also been applied in other fields (Bağcı Daş and Birant, 2021; Calderón et al., 2020). In light of these previous research, the ML approaches are implemented in this paper to predict the bending strength of the MVFT girder.

The high-performance construction material also gives rise to the development of the steel-concrete composite girders. Especially on the issue of ultra high-performance concrete (UHPC)-steel composite member, these researches mainly focus on the subjects: negative bending moment of steel-UHPFRC composite girders (Qi et al., 2020; Hamoda et al., 2017), flexural strength of UHPC-concrete composite members (Shirai et al., 2020). In addition, there are some findings on new type of composite girders, such as the post-installed shear connector aiming to strengthen composite bridge (Hällmark et al., 2019), bending capacity of U-shaped steel-concrete composite girders (Zhou et al., 2019) and straight-side U-shaped steel-encased concrete composite girders (Yan et al., 2021). Besides, some researchers have performed the dynamic analysis of the plate structure by using FE method (Das and Gonenli, 2022; Gonenli and Das, 2021; Das et al., 2020; Sahoo and Barik, 2020; Jafarpour and Khedmati, 2020).

In this paper, a series of pilot MVFT composite girders are established numerically and are analyzed theoretically to obtain the formula of the ultimate bending capacity, the capacity of MVFT girder is then predicted by the machine learning regressors (MLR). The accuracy of the two methods is verified by comparing the results of the fitting formula and the prediction results by machine learning approach. Therefore, this study combining FE method and MLR has reliable results and can avoid a large number of numerical calculations, which provides a new approach for MVFT girder's engineering design.

2 Configuration of the pilot MVFT girder

The steel girder and concrete plate of MVFT girder are both prefabricated in the mill, without secondary casting. The section near the support of MVFT girder is grouted. To reduce the dead weight, there is no grouted concrete in the mid-span section. The general section of MVFT girder is shown in Figure 1.

In this paper, 3:10 scaled pilot MVFT simply supported composite girder was investigated numerically. The reduced scale span of MVFT girder is 9m. The cross-section of the model is shown in Figure 2, and Figure 3 presents the detailed geometry of steel dowel. The overall and detailed finite element model are demonstrated in Figure 4 and Figure 5, respectively.

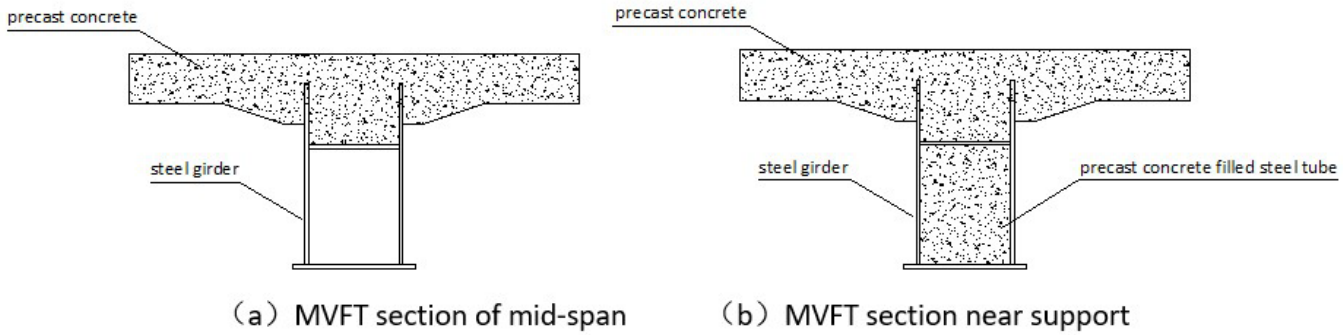

Figure 1 MVFT section.

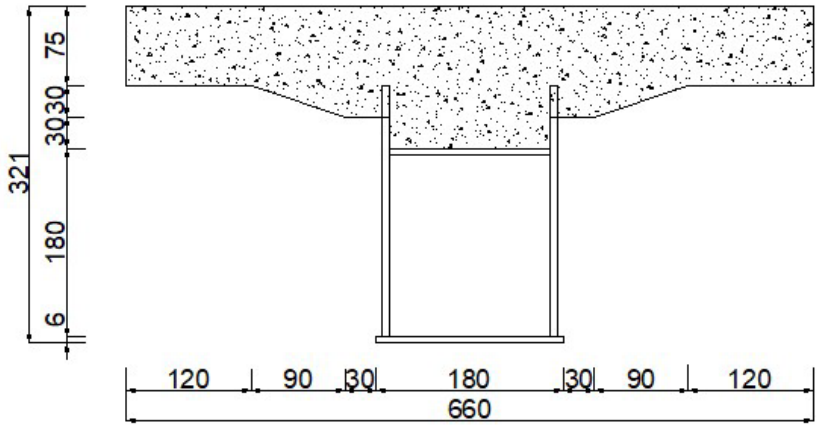

Figure 2 Geometric parameters of MVFT girder(unit:mm).

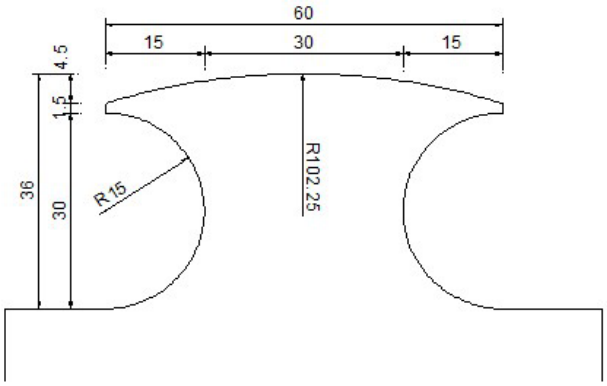

Figure 3 Details of steel dowel(unit:mm).

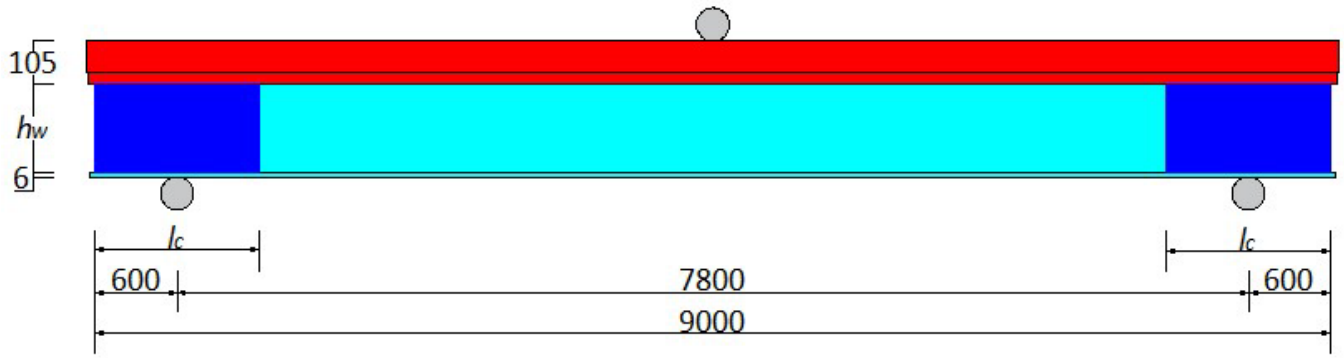

Figure 4 Elevation of pilot MVFT girder (unit:mm).

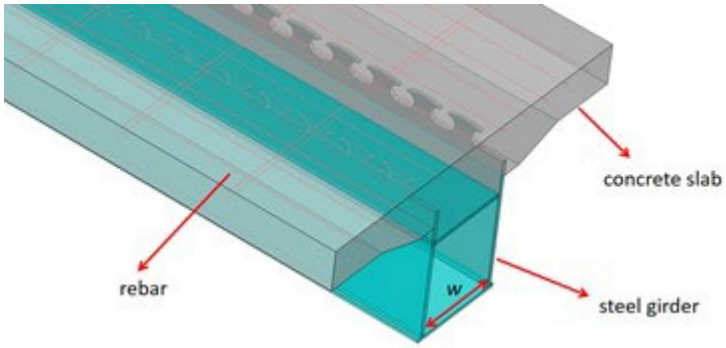

Figure 5 Details of FE model.

To explore the influence of web height(h_w), clear spacing between webs(w), and length of concrete filled steel tube(l_c) on the bending capacity of MVFT girders, the parametric studies are conducted based on the validated FE model as tabulated in Table 1. (Note: All dimensions in Table 1 are full-scale values.)

Table 1 Schemes for the parametric study.

Scheme No.	h_w(mm)	w(mm)	l_c(m)
NS1	700	452	0
NS2	700	452	3
NS3	700	452	4
NS4	700	452	5
NS5	700	467	0
NS6	700	467	3
NS7	700	467	4
NS8	700	467	5
NS9	700	482	0
NS10	700	482	3
NS11	700	482	4
NS12	700	482	5
NS13	700	497	0
NS14	700	497	3
NS15	700	497	4
NS16	700	497	5
NS17	700	512	0
NS18	700	512	3
NS19	700	512	4
NS20	700	512	5

Table 1 Continued...

Scheme No.	h_w(mm)	w(mm)	l_c(m)
NS21	800	452	0
NS22	800	452	3
NS23	800	452	4
NS24	800	452	5
NS25	800	467	0
NS26	800	467	3
NS27	800	467	4
NS28	800	467	5
NS29	800	482	0
NS30	800	482	3
NS31	800	482	4
NS32	800	482	5
NS33	800	497	0
NS34	800	497	3
NS35	800	497	4
NS36	800	497	5
NS37	800	512	0
NS38	800	512	3
NS39	800	512	4
NS40	800	512	5
NS41	900	452	0
NS42	900	452	3
NS43	900	452	4
NS44	900	452	5
NS45	900	467	0
NS46	900	467	3
NS47	900	467	4
NS48	900	467	5
NS49	900	482	0
NS50	900	482	3
NS51	900	482	4
NS52	900	482	5
NS53	900	497	0
NS54	900	497	3
NS55	900	497	4
NS56	900	497	5
NS57	900	512	0
NS58	900	512	3
NS59	900	512	4
NS60	900	512	5

In this paper, the ultimate load and bending strength of MVFT girder were obtained through the 3-point flexural test. And the failure mode of MVFT girder were identified by the concrete slab's load-strain curve and the steel girder's load-strain curve.

3 Numerical test and result

3.1 Validation of FE model

In the start of numerical test, the FE model was validated by the pull-out experimental data of composite dowels in UHPC slabs, which was conducted by Gallwoszus and Claßen (2015). The test steel dowels had a web thickness of 20 mm and were made of S460 structural steel. The dimensions of the puzzle-shaped steel dowel and the UHPC slab are shown in Figure 6, where h is the embedment depth of steel dowel.

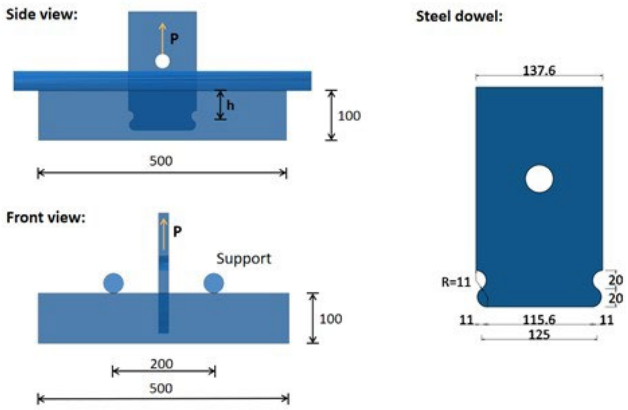

Figure 6 Dimensions of test specimen(unit:mm).

The FE analysis was performed in ABAQUS to simulate the pull-out test. The steel dowel and UHPC slab were discretized with a uniform mesh of solid elements C3D8R. Surface-to-surface contact was employed to describe the interaction between the steel dowel and UHPC slab. The surface of steel dowel and UHPC slab were chosen as the master surface and the slave surface, respectively. Contact properties were defined along with both the normal and tangential directions. The penalty friction algorithm with the friction coefficient of 0.3 was used to characterize the tangential behavior between the steel dowel and UHPC slab. Hard contact algorithm was employed in the normal direction. The numerical simulation results are demonstrated in Figure 7. The comparison between test and numerical simulation results is listed in Table 2. It can be found from Table 2 that the simulation results by FE agree with the test results.

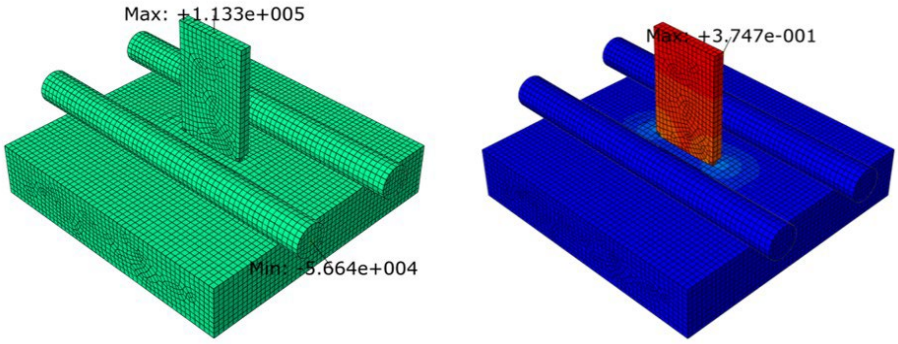

Figure 7 Results of numerical modeling.

Table 2 Comparison between the results obtained by numerical simulation (NS) and static pull-out tests.

h(mm)	Scheme No.	P_{max}(kN)	δ(mm)
60	Test1	118	0.35
	NS1	113.27	0.375
50	Test2	96	0.36
	NS2	99.63	0.362

3.2 Ultimate load of MVFT girder

Similarly with the previous validation model, the concrete slab, steel girders, stiffening ribs and concrete filled steel tube were simulated by three-dimensional eight-node solid elements (C3D8R) with one integration point. And three-dimensional two-node truss elements (T3D2) were used for the rebars in concrete slab. The loading device and supports were set as rigid bodies. The bilinear constitutive model was adopted for the steel with the value of yield strength(f_y) of 345MPa, Young's modulus (E_s) of 2.06x10^{5}MPa, and tangent modulus of strengthening stage of 0.01E_s. The material characteristics of concrete can be represented by the concrete damage plasticity (CDP) model in ABAQUS. The design value of concrete compressive strength(f_c) is 23.1MPa, the value of Young's modulus (E_c) is 3.42x10^{4}MPa.

According to the numerical simulation results, the *P*-δ curve is plotted in Figure 8, where *P* is the loading force, δ is the mid-span vertical deflection.

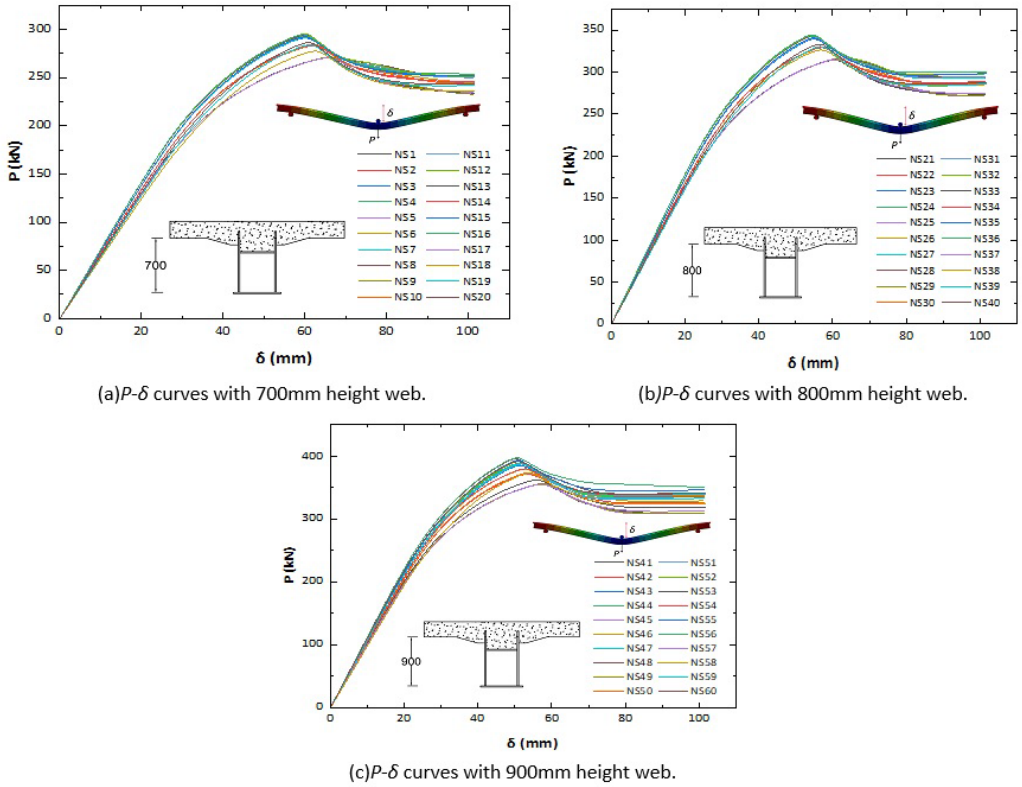

(a)*P*-δ curves with 700mm height web.

(b)*P*-δ curves with 800mm height web.

(c)*P*-δ curves with 900mm height web.

Figure 8 Load-deflection curves of MVFT girder.

To further exhibit the effect of *w* and l_c on the ultimate load(P_u) more directly, Table 3 summaries the results by controlling variables.

Table 3 Effect of *w* and l_c on the ultimate load.

Group No.	Groups of *w*		Group No.	Groups of l_c	
	Label	P_u(kN)		Label	P_u(kN)
1	NS1	270.54	2	NS1	270.54
	NS5	271.11		NS2	282.84
	NS9	271.48		NS3	291.06
	NS13	270.40		NS4	293.28
	NS17	270.34		NS5	271.11
	NS2	282.84		NS6	283.96
	NS6	283.96		NS7	291.99
	NS10	284.47		NS8	294.26
	NS14	283.86		NS9	271.48
	NS18	277.37		NS10	284.47
	NS3	291.06		NS11	293.00

Table 3 Continued...

Group No.	Groups of w		Group No.	Groups of l_c	
	Label	P_u(kN)		Label	P_u(kN)
	NS7	291.99		NS12	295.40
	NS11	293.00		NS13	270.40
	NS15	292.41		NS14	283.86
	NS19	283.93		NS15	292.41
	NS4	293.28		NS16	294.67
	NS8	294.26		NS17	270.34
	NS12	295.40		NS18	277.37
	NS16	294.67		NS19	283.93
	NS20	286.12		NS20	286.12
	NS21	314.29		NS21	314.29
	NS25	315.40		NS22	329.15
	NS29	315.33		NS23	339.50
	NS33	314.90		NS24	342.74
	NS37	314.63		NS25	315.40
	NS22	329.15		NS26	329.48
	NS26	329.48		NS27	340.77
	NS30	330.27		NS28	343.67
	NS34	329.35		NS29	315.33
	NS38	326.31		NS30	330.27
	NS23	339.50		NS31	340.94
	NS27	340.77		NS32	344.47
	NS31	340.94		NS33	314.90
	NS35	340.70		NS34	329.35
	NS39	330.46		NS35	340.70
	NS24	342.74		NS36	344.39
	NS28	343.67		NS37	314.63
	NS32	344.47		NS38	326.31
	NS36	344.39		NS39	330.46
	NS40	332.84		NS40	332.84
	NS41	355.35		NS41	355.35
	NS45	356.56		NS42	371.66
	NS49	356.78		NS43	385.57
	NS53	362.55		NS44	388.46
	NS57	354.83		NS45	356.56
	NS42	371.66		NS46	379.90
	NS46	379.90		NS47	387.73
	NS50	374.19		NS48	396.18
	NS54	380.32		NS49	356.78
	NS58	372.87		NS50	374.19
	NS43	385.57		NS51	388.73
	NS47	387.73		NS52	392.33
	NS51	388.73		NS53	362.55
	NS55	393.64		NS54	380.32
	NS59	388.21		NS55	393.64
	NS44	388.46		NS56	397.64
	NS48	396.18		NS57	354.83
	NS52	392.33		NS58	372.87
	NS56	397.64		NS59	388.21
	NS60	391.91		NS60	391.91

It can be observed from Figure 8, when the h_w increases from 700mm to 800mm and 900mm, the ultimate load (P_u) shows an obvious increase. As shown in Table 3, with the increase of w, the P_u increases first and then decreases overall; and the P_u increases gradually with increasing l_c.

3.3 Failure mode of MVFT girder

The bending failure modes of steel-concrete composite girders with full shear connection are mainly classified into concrete slab compressive failure and steel girder tensile failure. In this paper, the failure mode is determined under the assumption of plastic theory. The concrete will be crushed when the maximum compressive strain of concrete slab($\varepsilon_{cc,max}$) exceeds the ultimate compressive strain of concrete(ε_{cu}), and ε_{cu} is set to be 0.0033, according to the *Code for design of concrete structures* (GB 50010-2010); the steel will be yielded when the maximum tensile strain of steel girder($\varepsilon_{st,max}$) exceeds the ultimate tensile strain of steel(ε_{su}), and $\varepsilon_{su}=15\varepsilon_y$, which is defined by the *Eurocode 3*. For the steel involved in the analysis, ε_{su} is 0.02803. In order to discuss the failure mode of MVFT girder, load-concrete slab compressive strain curves (P-ε_{cc} curves) and load-steel girder tensile strain curves (P-ε_{st} curves) are plotted in Figure 9 and Figure 10. As shown in Figure 9 and Figure 10, $\varepsilon_{cc,max}$ exceeds 0.0033, and ε_{su} is less than 0.02803, when the web height of MVFT girders is 700mm, 800mm and 900mm, respectively. Therefore, the failure mode of MVFT composite girder is due to the concrete slab's crush. The compression damage of concrete slab is shown in Figure 11, and the tensile strain of steel girder corresponding is shown in Figure 12, while steel girder has turned into plastic stage.

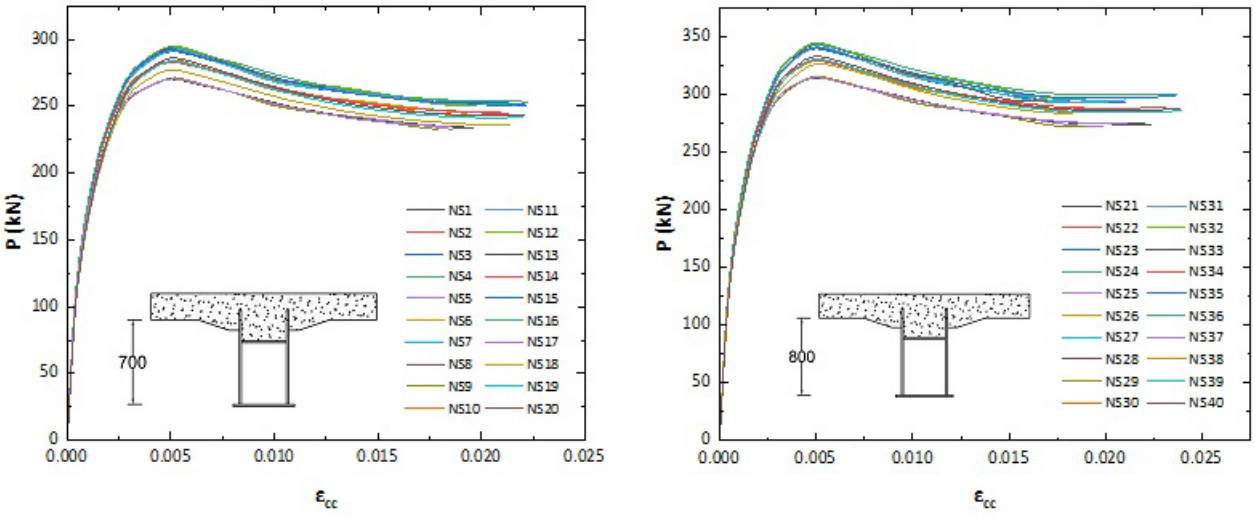

(a)P-ε_{cc} curves with 700mm height web.

(b)P-ε_{cc} curves with 800mm height web.

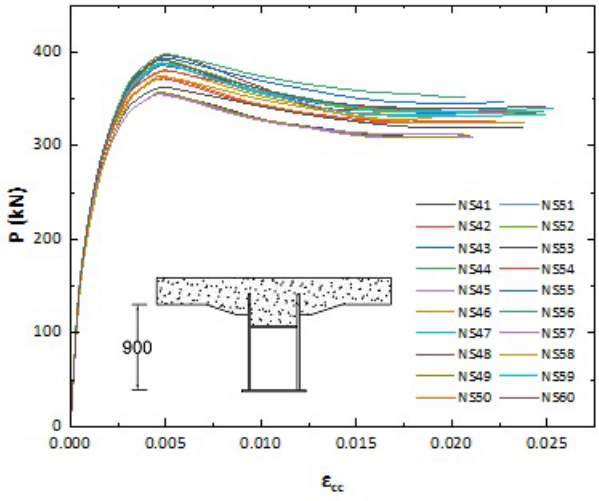

(c)P-ε_{cc} curves with 900mm height web.

Figure 9 Load-concrete slab's compressive strain curves.

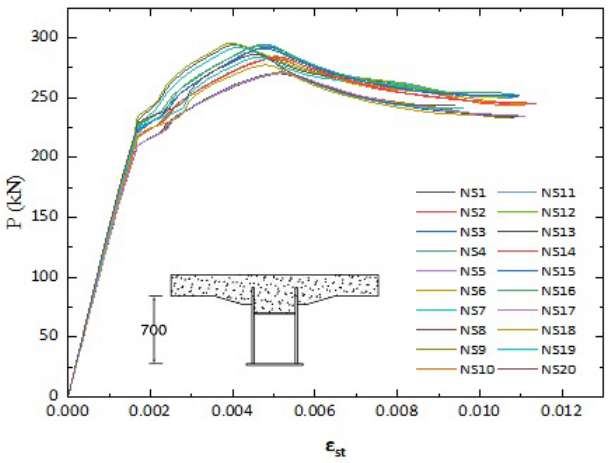

(a)P-ε_{st} curves with 700mm height web.

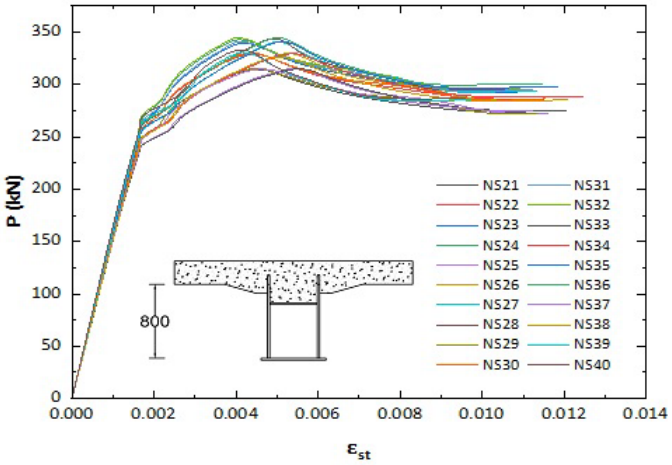

(b)P-ε_{st} curves with 800mm height web.

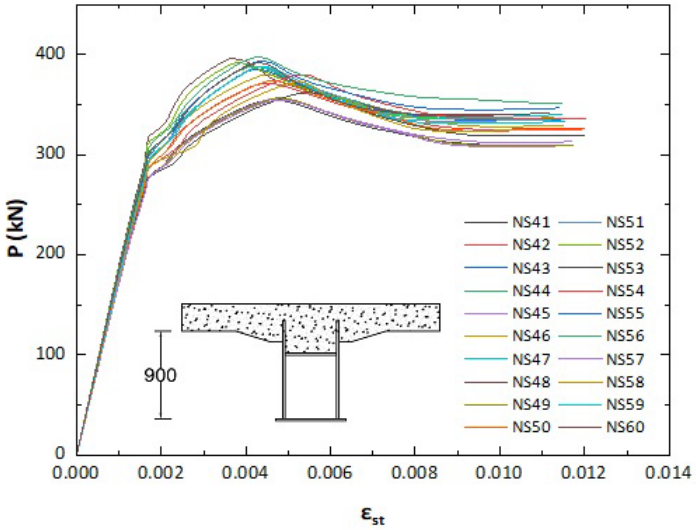

(c)P-ε_{st} curves with 900mm height web.

Figure 10 Load-steel girder's tensile strain curves.

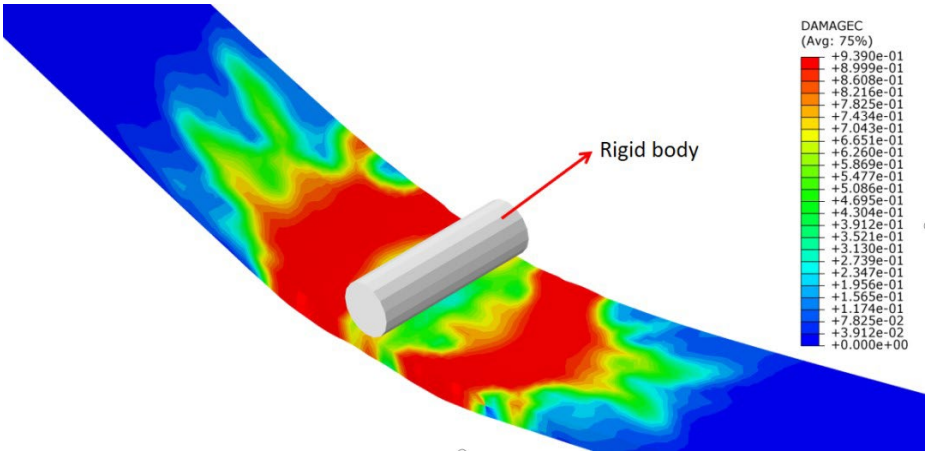

Figure 11 Contour plot of concrete slab compression damage.

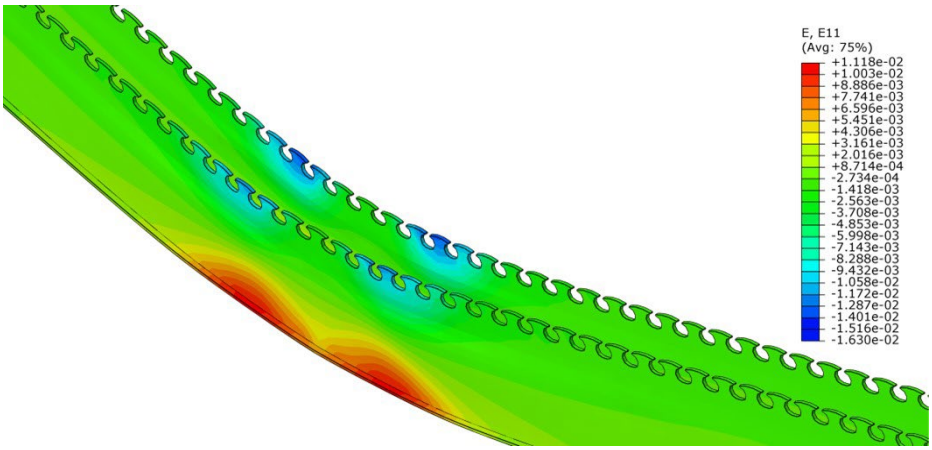

Figure 12 Tensile strain of the steel girder corresponding to the concrete slab compression damage.

4 Formula of ultimate bending strength

For MVFT girder, there is no design formula for its ultimate bending strength at present, while the design formulas for ultimate flexural capacity of conventional steel-concrete composite girder under the assumption of plastic theory are provided by the *Code for design of composite structures* (JGJ 138-2016) and the *Standard for design of steel structures* (GB 50017-2017). There is no essential or formal difference between the two formulas. Considering that the steel girder is inserted into the concrete and cooperates with the concrete, the concrete will be strengthened based on the formula from the code (JGJ 138-2016, GB 50017-2017). Therefore, a concrete strengthening coefficient(α) is proposed to modify the existing code formula. With the assumption that the plastic neutral axis is located in the steel girder, and the calculation model is shown in Figure 13.

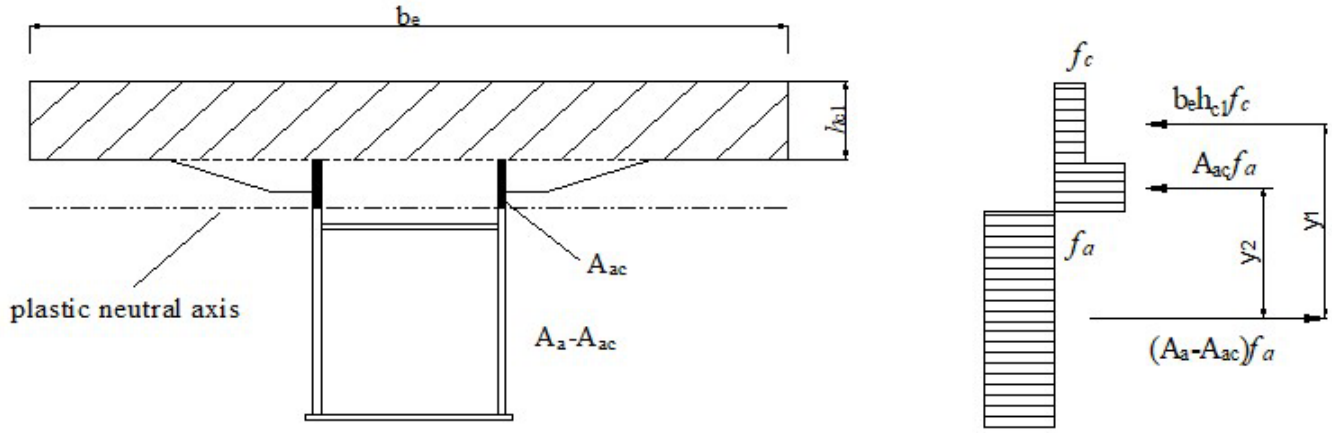

Figure 13 Calculation model of ultimate bending strength.

The calculation formula for ultimate bending capacity of MVFT girder is proposed by Equation (1):

$$M \le \alpha b_e f_c h_{c1} y_1 + A_{ac} f_a y_2 \tag{1}$$

where α is the concrete strengthening coefficient, f_c is the design value of concrete compressive strength, f_a is the design value of steel compressive and tensile strength, b_e is the effective width of MVFT composite girder, h_{c1} is the thickness of concrete slab, y_1 is the distance between steel girder's tensile centroid and slab's compressive centroid, y_2 is the distance between steel girder's tensile centroid and its compressive centroid, A_{ac} is the compressive area of steel girder, A_a is the area of steel girder.

The ultimate bending moments of MVFT girders were calculated by FEM(M_{NSU}) , design formula (M_{codeU}) are presented in Table 4.

Table 4 Comparison of FEM and design formula predicted ultimate moment capacity of MVFT girders.

Scheme No.	M_{NSU}(kN·m)	M_{codeU}(kN·m)	M_{NSU}/M_{codeU}
NS1	248.3	208.82	1.19
NS2	246.8	208.82	1.18
NS3	244.8	208.82	1.17
NS4	243.9	208.82	1.17
NS5	249.3	209.80	1.19
NS6	248	209.80	1.18
NS7	245.6	209.80	1.17
NS8	244.5	209.80	1.17
NS9	250.2	210.78	1.19
NS10	248.3	210.78	1.18
NS11	246.1	210.78	1.17
NS12	244.9	210.78	1.16
NS13	246.9	211.76	1.17
NS14	246.2	211.76	1.16
NS15	243.7	211.76	1.15
NS16	243	211.76	1.15
NS17	246.6	212.74	1.16
NS18	239.8	212.74	1.13
NS19	238.9	212.74	1.12
NS20	237.8	212.74	1.12
NS21	287.8	245.32	1.17
NS22	285.1	245.32	1.16
NS23	285	245.32	1.16
NS24	287.3	245.32	1.17
NS25	298.9	246.36	1.21
NS26	297.6	246.36	1.21
NS27	294.7	246.36	1.20
NS28	293.3	246.36	1.19
NS29	289.2	247.41	1.17
NS30	288.4	247.41	1.17
NS31	285.4	247.41	1.15
NS32	284.3	247.41	1.15
NS33	297.3	248.45	1.20
NS34	295.7	248.45	1.19
NS35	292.7	248.45	1.18
NS36	291.5	248.45	1.17
NS37	287.4	249.49	1.15
NS38	290.5	249.49	1.16
NS39	279	249.49	1.12
NS40	277.8	249.49	1.11
NS41	355.8	283.80	1.25
NS42	351.8	283.80	1.24
NS43	347.7	283.80	1.23
NS44	346.2	283.80	1.22
NS45	355	284.91	1.25
NS46	354.4	284.91	1.24
NS47	349.1	284.91	1.23
NS48	348.6	284.91	1.22
NS49	356.2	286.01	1.25
NS50	353.7	286.01	1.24
NS51	349.3	286.01	1.22
NS52	347.5	286.01	1.21
NS53	355.1	287.11	1.24
NS54	353.9	287.11	1.23
NS55	349.5	287.11	1.22
NS56	348.4	287.11	1.21
NS57	353.1	288.22	1.23
NS58	346.2	288.22	1.20
NS59	346.8	288.22	1.20
NS60	345.2	288.22	1.20

As shown in Table 4, the length of grouted concrete in the girder (l_c) has little influence on the ultimate flexural strength of MVFT girder. Therefore, all 60 groups of M_{NSU} can be used to fit the proposed correction formula of MVFT girder, and the concrete strengthening coefficient α=1.221 was obtained. In terms of the coefficient of determination R^2=0.9483, the fitting results were precise. In addition, it can be seen from Table 4 that the calculation results of the ultimate moment resistance using the present code are slightly conservative.

5 Ultimate bending strength by Machine Learning

In the calculation formula for ultimate bending capacity of MVFT girder, A_{ac}, y_1, y_2 are variables that have influence on the M_{NSU}. Therefore, the three factors that A_{ac}, y_1, y_2 are determined as the independent variables of the prediction model while the corresponding M_{NSU} is set as the dependent variable of the model. A total of 60 samples were listed from the former study. 48 sets of samples are randomly selected as training set, and the remaining 12 sets of sample data served as the test part for the reliability of prediction models. Considering that the units of different uncertain parameters and the numerical magnitude may have different degrees of influence on the prediction results, all the extracted samples are normalized and collated. The normalization formula is expressed in Equation (2).

$$P_i = \frac{x_i - x_{\min}}{x_{\max} - x_{\min}} \tag{2}$$

where P_i is the normalized data of a variable x_i in the training sample; x_{min} is the minimum value of that group of data in the sample; x_{max} is the maximum value of that group of data in the sample.

5.1 BP neural network-based ultimate bending strength prediction model

BP neural network is a multi-layer feed-forward network trained by back propagation of error. The single hidden layer network structure is chosen for the prediction model in this paper, due to the fact that the neural network can approximate any complex continuous mapping if the single hidden layer feed-forward neural network is continuous and the transfer function is sigmoid (Hornik et al., 1989). It will lead to underfitting or overfitting respectively because of deficiency or surplus hidden layer neurons. And the error of the prediction model can be minimized when the number of hidden layer neurons is 3 according to a large number of artificial neural network modeling experience and computational data comparison results. Hence, the number of hidden layer neurons is determined to be 3 here, and the flow chart of the BP neural network is shown in Figure 14.

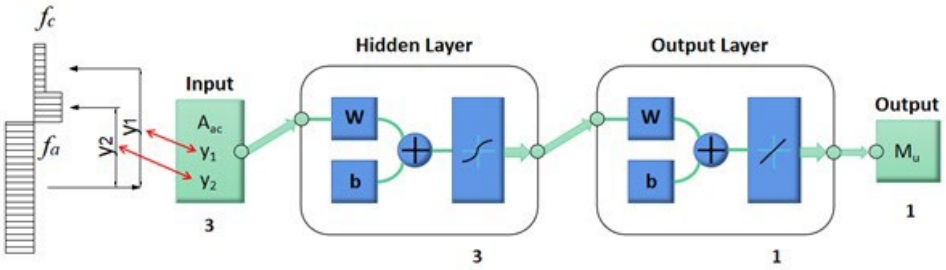

Figure 14 Flow chart of the BP neural network

This model applies the L-M algorithm to optimize the search direction of the network weight vector so that the network quickly approaches the objective function. The iterative equation of the L-M algorithm is expressed in Equation (3), (4).

$$x^{(k+1)} = x^k - [J^T J + uJ]^{-1} J^T e \tag{3}$$

$$H = J^T J \tag{4}$$

where $x^{(k)}$, $x^{(k+1)}$ are the vectors composed of weights and thresholds among the layers in the k^{th} and $k+1^{th}$ iterations of the neural network, respectively; e is the error vector of each layer of the network; u is the coefficient, Equation (4) is the Newton method when u is 0; Equation (4) is the gradient descent method; H is the Hessian matrix when u is large.

The network learning rate is set to 0.01 and the maximum training round is 1000 times. In order to ensure the general vadility of the prediction results, the BP neural network is randomly performed five times. Some of the results predicted by BP neural network with MATLAB are shown in Table 5.

Table 5 BP neural network prediction results.

Group No.	Test No.	M_{pre}	M_{NSU}	relative error
1	Test1	245.1	247.3	0.0090
	Test2	291.3	290.5	0.0027
	Test3	351.4	348.4	0.0085
	Test4	292.0	289.2	0.0098
	Test5	245.8	248.3	0.0100
	Test6	351.1	348.6	0.0073
	Test7	351.3	353.7	0.0069
	Test8	291.3	287.4	0.0135
	Test9	292.0	284.3	0.0272
	Test10	351.4	345.2	0.0181
	Test11	291.6	291.5	0.0005
	Test12	246.6	245.6	0.0039
2	Test1	288.28	288.4	0.0004
	Test2	246.93	249.3	0.0095
	Test3	245.28	246.9	0.0066
	Test4	246.09	248.3	0.0089
	Test5	287.51	295.7	0.0277
	Test6	287.51	292.7	0.0177
	Test7	350.72	356.2	0.0154
	Test8	287.51	297.3	0.0329
	Test9	244.48	239.8	0.0195
	Test10	350.47	348.6	0.0054
	Test11	286.78	287.4	0.0022
	Test12	350.47	355	0.0128
3	Test1	244.58	246.9	0.0094
	Test2	290.78	293.3	0.0086
	Test3	238.14	239.8	0.0069
	Test4	238.14	246.6	0.0343
	Test5	247.17	246.8	0.0015
	Test6	290.78	294.7	0.0133
	Test7	248.44	245.6	0.0116
	Test8	348.84	355.8	0.0196
	Test9	247.17	243.9	0.0134
	Test10	247.81	246.1	0.0069
	Test11	248.44	244.5	0.0161
	Test12	247.17	248.3	0.0045
4	Test1	288.78	293.3	0.0154
	Test2	286.83	295.7	0.0300
	Test3	350.56	347.5	0.0088
	Test4	348.96	346.2	0.0080
	Test5	289.77	287.3	0.0086
	Test6	288.78	297.6	0.0296
	Test7	288.78	298.9	0.0339
	Test8	349.74	353.9	0.0118
	Test9	350.56	353.7	0.0089
	Test10	287.80	284.3	0.0123
	Test11	244.43	246.6	0.0088
	Test12	287.80	288.4	0.0021
5	Test1	349.89	346.8	0.0089
	Test2	244.74	243.7	0.0043
	Test3	289.53	285.4	0.0145
	Test4	349.80	348.4	0.0040
	Test5	289.53	284.3	0.0184
	Test6	349.61	349.1	0.0015
	Test7	349.89	353.1	0.0091
	Test8	288.41	285.1	0.0116
	Test9	290.12	292.7	0.0088
	Test10	245.26	249.3	0.0162
	Test11	244.55	246.6	0.0083
	Test12	349.61	354.4	0.0135

5.2 LSSVM-based ultimate bending strength prediction model

The primary principle of least squares support vector machine (LSSVM) regression is to map the input data to a high-dimensional feature space through certain nonlinear mapping, and then construct the optimal linear regression equation in the high-dimensional space. The LSSVM approach's advantages include high accuracy (Wang and Hu, 2005), a fast-solving speed, and consumes less computational resources. According to the principle of Structure Risk Minimization (SRM), the training objective of LSSVM can be expressed as Equation (5), (6).

$$\min = \frac{1}{2}\|\omega\|^2 \frac{1}{2}\gamma\sum_{i=1}^{l} e_i^2 \tag{5}$$

$$s.t.\ \ \omega^T\varphi(x_i) + b + e_i = y_i \quad i = 1,2,\ldots,l \tag{6}$$

where γ is the regularization parameter that controls the degree of penalty on the error; ω is the weight vector; $\varphi(x_i)$ is the kernel function; b is the offset; and e_i is the error variable.

The normalized data was used to build a system numerical model in MATLAB for simulation analysis, where LSSVM offline training was implemented with algorithmic programming. To ensure the general vadility of the prediction results, the LSSVM is randomly performed five times as well. The predicted values are listed in Table 6.

Table 6 LSSVM prediction results.

Group No.	Test No.	M_{pre}	M_{NSU}	relative error
1	Test1	349.90	355	0.0144
	Test2	298.19	294.7	0.0118
	Test3	250.25	246.1	0.0168
	Test4	298.19	293.3	0.0167
	Test5	250.25	244.9	0.0218
	Test6	347.40	346.8	0.0017
	Test7	240.56	246.6	0.0245
	Test8	351.64	349.3	0.0067
	Test9	240.56	237.8	0.0116
	Test10	245.04	246.9	0.0075
	Test11	284.39	287.4	0.0105
	Test12	284.39	279	0.0193
2	Test1	286.30	288.4	0.0073
	Test2	246.03	249.3	0.0131
	Test3	244.30	246.9	0.0105
	Test4	247.07	248.3	0.0050
	Test5	291.50	295.7	0.0142
	Test6	291.50	292.7	0.0041
	Test7	350.17	356.2	0.0169
	Test8	291.50	297.3	0.0195
	Test9	241.10	239.8	0.0054
	Test10	351.75	348.6	0.0090
	Test11	282.43	287.4	0.0173
	Test12	351.75	355	0.0092
3	Test1	352.33	349.1	0.0092
	Test2	288.88	285.4	0.0122
	Test3	352.12	349.3	0.0081
	Test4	345.71	353.1	0.0209
	Test5	291.51	297.3	0.0195

Table 6 Continued...

Group No.	Test No.	M_{pre}	M_{NSU}	relative error
	Test6	352.48	348.4	0.0117
	Test7	351.36	346.2	0.0149
	Test8	288.88	284.3	0.0161
	Test9	248.09	246.1	0.0081
	Test10	291.51	292.7	0.0041
	Test11	291.51	295.7	0.0142
	Test12	247.54	245.6	0.0079
4	Test1	245.89	249.3	0.0137
	Test2	244.70	246.9	0.0089
	Test3	247.31	248.3	0.0040
	Test4	352.76	349.1	0.0105
	Test5	241.62	238.9	0.0114
	Test6	244.70	243	0.0070
	Test7	354.58	349.5	0.0145
	Test8	354.58	348.4	0.0177
	Test9	352.87	347.5	0.0155
	Test10	245.36	248.3	0.0118
	Test11	349.37	346.8	0.0074
	Test12	349.37	345.2	0.0121
5	Test1	294.49	295.7	0.0041
	Test2	241.34	239.8	0.0064
	Test3	349.02	353.9	0.0138
	Test4	355.01	348.6	0.0184
	Test5	246.54	244.8	0.0071
	Test6	355.01	349.1	0.0169
	Test7	294.49	291.5	0.0103
	Test8	351.04	347.7	0.0096
	Test9	349.02	355.1	0.0171
	Test10	286.69	288.4	0.0059
	Test11	355.01	354.4	0.0017
	Test12	294.87	298.9	0.0135

The mean absolute percentage error (MAPE) and root mean square error (RMSE) are assigned to measure the accuracy of the prediction model for training and prediction of existing data. In the light of the error judgment rule, the prediction effect of the model is more accurate as MAPE and RMSE get closer to zero. Defining the predicted output value to be Pre_i, the true value to be P, then the MAPE and RMSE are calculated as follows in Equation (7), (8).

$$MAPE = \left(\frac{1}{m}\sum_{k=1}^{m}\frac{\left|\Pr e_i - P\right|}{\Pr e_i}\right)\times 100\% \tag{7}$$

$$RMSE = \sqrt{\frac{1}{m}\sum_{k=1}^{m}(\Pr e_i - P)^2} \tag{8}$$

The error analysis of the prediction results by the above equations is listed in Table 7.

Table 7 Error comparison of two ML models.

ML model	Group No.	Maximum relative error	MAPE	RMSE
BP(L-M)	1	0.0272	0.0095	0.5454
	2	0.0329	0.0132	0.7386
	3	0.0343	0.0122	0.6068
	4	0.0339	0.0148	0.8233
	5	0.0184	0.0099	0.5012
	average	0.0293	0.0119	0.6431
LSSVM	1	0.0245	0.0136	1.1766
	2	0.0195	0.011	1.0519
	3	0.0209	0.0122	1.2067
	4	0.0177	0.0112	1.0754
	5	0.0184	0.0104	1.1281
	average	0.0202	0.0117	1.1277

As shown in Table 7, it is clear that the mean value of MAPE and RMSE of the two prediction models are both close to 0, but the prediction model based on the BP neural network obtains smaller mean MAPE and RMSE, while the prediction model based on LSSVM obtains smaller mean maximum relative error. And both their results show high precision and strong stability.

5.3 BP neural network-based ultimate bending strength extrapolation prediction model

It can be seen from Table 5, 6 and 7 that the two ML models can fit the historical data with high accuracy, in general, the BP neural network model is more precise than LSSVM. On this basis, the BP model is developed to predict the ultimate bending capacity of MVFT girders with new section, and to compare the calculation results of the fitting formula. The section properties of 30 meters MVFT girder are shown in Table 8. The ultimate bending strength prediction of 30 meters MVFT girder by BP neural network model (M_{EU}) and the formula (M_{FU}) are listed in Table 9 and have been compared, which correlates well with each other and validates their precision. Assuming the accuracy of the formula, it is employed to calculate the ultimate flexural capacity of MVFT girder with other span length, without using the BP neural network to make predictions. Then, the fitting formula is used to predict the ultimate flexural strength of 40 meters MVFT girder, and the results are shown in Table 10. (Note: Where b is the width of concrete slab, h_{c1} is the height of concrete slab, h_w is the height of web, t_w is the thickness of web, w_f is the width of flange, t_f is the thickness of flange, w is the clear spacing between webs.)

Table 8 Section Properties of 30 meters MVFT girder.

Section No.	Section Properties								
	b(mm)	h_{c1}(mm)	h_w(mm)	t_w (mm)	w_f (mm)	t_f (mm)	w (mm)	f_a (MPa)	f_c (MPa)
Sec1	2200	250	700	24	600	20	497	295	23.1
Sec2	2200	250	800	24	600	20	482	295	23.1
Sec3	2200	250	900	24	600	20	467	295	23.1
Sec4	2200	250	700	24	600	20	472	295	23.1
Sec5	2200	250	800	24	600	20	492	295	23.1
Sec6	2200	250	900	24	600	20	432	295	23.1

Table 9 Ultimate bending strength prediction of 30 meters MVFT girder.

Section No.	M_{EU} (kN·m)						M_{FU} (kN·m)
	1	2	3	4	5	average	
Sec1	9085	9097.3	9119.9	9049	9122.5	9094.74	9193.69
Sec2	10763	11030	10715	10519	10796	10764.6	10697.03
Sec3	12671	12927	12877	12905	12966	12869.2	12266.75
Sec4	9089.2	9078.5	9087.5	9069.1	9095.2	9083.9	9126.74
Sec5	10588	10686	10870	10632	10760	10707.2	10725.28
Sec6	12959	12939	12789	12970	12958	12923	12162.69

Table 10 Ultimate bending strength prediction of 40 meters MVFT girder.

Pre No.	Section Properties									M_{FU} (kN·m)
	b(mm)	h_{c1}(mm)	h_w(mm)	t_w (mm)	w_f (mm)	t_f (mm)	w (mm)	f_a (MPa)	f_c (MPa)	
Pre1	2200	300	1150	24	600	20	512	295	23.1	17195.61
Pre2	2200	300	1100	24	600	20	452	295	23.1	18402.37
Pre3	2200	300	1200	24	600	20	482	295	23.1	19299.22

6 CONCLUSION

In this paper, a series of pilot MVFT composite girders are established numerically and the finite element models are validated against background experiment. The ultimate bending capacity and failure mode of MVFT girder are studied through the verified numerical models, the capacity of MVFT girder is then predicted by MLR. The following conclusions are drawn:

1. Owing to the steel web of MVFT girder embedding in concrete, the concrete resistance part will be reinforced compared with typical steel-concrete composite girder. Therefore, a concrete strengthening coefficient is proposed based on the existing code formula, and the formula of ultimate bending strength of MVFT girder is proposed accordingly. According to the fitting results, the concrete strengthening coefficient α=1.221 has been obtained. In terms of the coefficient of determination R^2=0.9483, the fitting formula is precise.
2. With the ascending clear spacing between webs, the ultimate load shows a trend of initial increasing and then decreasing. The rule can be used as a reference for the preliminary section design of MVFT girder. Under the assumption of plastic theory, both the load-strain curves of concrete and steel girder disclose that: the failure of MVFT girder under bending is owing to the concrete crushing.
3. The two ML models, BP neural network and LSSVM, can fit the historical data of the ultimate bending moment of the MVFT girder with high precision: The mean maximum relative errors of the two ML models are less than 3%, and the mean values of MAPE and RMSE of the two ML models are close to 0. On this basis, the BP neural network is developed to predict the ultimate bending capacity of MVFT girders with new section, and the prediction results are in good agreement with the calculation results of the fitting formula, which validates their accuracy. The ML models are capable of an accurate prediction of the strength of MVFT section with a sufficient database, which is essential for the steel-concrete composite bridge design. Furthermore, this approach combining FE method and MLR provides a reliable result and can avoid a large number of numerical simulations, which is highly efficient in engineering design.

ACKNOWLEDGEMENTS

This research is financially supported by Elite Scholar Program of Northwest A&F University (Grant No. Z111022001).

Author's Contributions: Conceptualization, ZH Xiong; Methodology, ZH Xiong and JW Li; Investigation, JW Li, HD Zhu, XY Liu; Writing - original draft, JW Li and ZX Liang; Writing - review & editing, ZH Xiong and JW Li; Supervision, ZH Xiong.

Editor: Rogério José Marczak

References

Abdeljaber, O., Avci, O., Kiranyaz, M.S., Boashash B., Sodano, H., Inman, D.J. (2018). 1-D CNNs for structural damage detection: Verification on a structural health monitoring benchmark data. Neurocomputing. 275: 1308-1317.

Bağcı Daş, D., Birant, D. (2021). Ordered physical human activity recognition based on ordinal classification. Turkish Journal of Electrical Engineering & Computer Sciences. 29: 2416 -2436

Berthellemy, J., Seidl, G., Lorenc, W. (2018). Recent structures and bridges built with the CL steel-concrete connection. DOI: 10.2749/nantes.2018.s2-51

Calderón M., Aguilar W.G., Merizalde D. (2020) Visual-Based Real-Time Detection Using Neural Networks and Micro-UAVs for Military Operations. In: Rocha Á., Paredes-Calderón M., Guarda T. (eds) Developments and Advances in Defense and Security. MICRADS 2020. Smart Innovation, Systems and Technologies, vol 181. Springer, Singapore.

Chen J., Li J., Xiong Z., Li J., Zhang H. (2021). Inspection of bridge damage in Maduo Earthquake and its effect on design scheme of bridge in cold region. Journal of Water Resources and Architectural Engineering 19(05): 99-104. (in Chinese). DOI: 10.13140/RG.2.2.19836.46720

Das, O., Gonenli, C. (2022). The Impact of the Cracks on the Harmonic Response of Stiffened Steel Plates. Latin American Journal of Solids and Structures. 19(2): e427. DOI: 10.1590/1679-78256790

Das, O., Ozturk, H., Gonenli, C. (2020). Finite element vibration analysis of laminated composite parabolic thick plate frames. Steel and Composite Structures. 35(1):43-59. DOI: 10.12989/scs.2020.35.1.043

Gallwoszus, J. and Claßen, M. (2015). Ermüdung von Verbunddübelleisten in UHPC unter zyklischer Pull-out-Beanspruchung. Bautechnik, 92(7):509-521.

Gonenli, C., Das, O. (2021). Effect of crack location on buckling and dynamic stability in plate frame structures. Journal of the Brazilian Society of Mechanical Sciences and Engineering. 43:31. DOI:10.1007/s40430-021-03032-2.

Hakim, S. J. S., Razak, H. A. (2013). Structural damage detection of steel bridge girder using artificial neural networks and finite element models. Steel Compos. Struct 14(4): 367-377.

Hällmark, R., Collin, P., and Hicks, S. J. (2019). Post-installed shear connectors: Push-out tests of coiled spring pins vs. headed studs. Journal of Constructional Steel Research, 161, 1-16.

Hamoda, A., Hossain, K. M. A., Sennah, K., Shoukry, M., Mahmoud, Z. (2017). Behaviour of composite high performance concrete slab on steel I-beams subjected to static hogging moment. Engineering Structures 140: 51-65.

Harnatkiewicz, P., Kopczyński, A., Kożuch, M., Lorenc, W., Rowiński, S. (2011). Research on fatigue cracks in composite dowel shear connection. Engineering Failure Analysis 18(5): 1279-1294.

Hechler, O., Berthellemy, J., Lorenc, W., Seidl, G., & Viefhues, E. (2011). Continuous shear connectors in bridge construction. In Composite Construction in Steel and Concrete VI (pp.78-91). https://ascelibrary.org/doi/abs/10.1061/41142(396)7

Hornik, K., Stinchcombe, M., White, H. (1989). Multilayer feedforward networks are universal approximators. Neural networks 2(5): 359-366.

Jafarpour, S., Khedmati, M.R. (2020). Vibration analysis of stiffened plates with initial geometric imperfections. Proceedings of the Institution of Mechanical Engineers, Part M: Journal of Engineering for the Maritime Environment. 235(2): 521-531. DOI: 10.1177/1475090220967520

Kołakowski, T. and Lorenc, W. (2015). Bridges by VFT method in Poland: state-of-the-art. In Economical Bridge Solutions based on innovative composite dowels and integrated abutments (pp. 111-131).

Li, S., Liew, J. R., Xiong, M. X. (2021). Prediction of fire resistance of concrete encased steel composite columns using artificial neural network. Engineering Structures, 245, 112877. https://doi.org/10.1016/j.engstruct.2021.112877

Liang, Q. Q., Uy, B., Bradford, M. A., Ronagh, H. R. (2005). Strength analysis of steel–concrete composite beams in combined bending and shear. Journal of Structural Engineering 131(10): 1593-1600.

Liu, J., Ding, F. X., Liu, X. M., Yu, Z. W., Tan, Z., Huang, J. W. (2019). Flexural capacity of steel-concrete composite beams under hogging moment. Advances in Civil Engineering, 2019. https://doi.org/10.1155/2019/3453274

Liu, Y., Xiong, Z., Luo, Y., Cheng, G., Liu, G., Yang, J. (2015). Double-composite rectangular truss bridge and its joint analysis. Journal of Traffic and Transportation Engineering (English Edition) 2(4): 249-257.

Petzek, E. and Bancila, R. (2010). EFFICIENT SOLUTIONS FOR COMPOSITE BRIDGES. International Scientific Conference CIBv2010, Brasov.

Qi, J., Cheng, Z., Wang, J., Tang, Y. (2020, April). Flexural behavior of steel-UHPFRC composite beams under negative moment. In Structures (Vol. 24, pp. 640-649). Elsevier. https://doi.org/10.1016/j.istruc.2020.01.022

Ryu, H. K., Youn, S. G., Bae, D., Lee, Y. K. (2006). Bending capacity of composite girders with Class 3 section. Journal of Constructional Steel Research 62(9): 847-855.

Sahoo, P.R., Barik, M. (2020). Free Vibration Analysis of Stiffened Plates. Journal of Vibration Engineering & Technologies. 8: 869–882. DOI:10.1007/s42417-020-00196-4

Shirai, K., Yin, H., Teo, W. (2020, February). Flexural capacity prediction of composite RC members strengthened with UHPC based on existing design models. In Structures(Vol. 23, pp. 44-55). Elsevier. https://doi.org/10.1016/j.istruc.2019.09.017

Svensson, H. (2013). Cable-stayed bridges: 40 years of experience worldwide. John Wiley & Sons.

Tadesse, Z., Patel, K. A., Chaudhary, S., Nagpal, A. K. (2012). Neural networks for prediction of deflection in composite bridges. Journal of Constructional Steel Research 68(1): 138-149.

Tan, Z. X., Thambiratnam, D. P., Chan, T. H., Gordan, M., Abdul Razak, H. (2020). Damage detection in steel-concrete composite bridge using vibration characteristics and artificial neural network. Structure and Infrastructure Engineering 16(9): 1247-1261.

Wang, H. and Hu, D. (2005, October). Comparison of SVM and LS-SVM for regression. In 2005 International Conference on Neural Networks and Brain (Vol. 1, pp. 279-283). IEEE. DOI: 10.1109/ICNNB.2005.1614615

Xiong, Z. (2021). A prefabricated MVFT composite girder suitable for small-span bridges. 4th International Conference on Structural Integrity. Portugal. https://www.youtube.com/watch?v=YWBs4MceyZI&t=11s

Xiong, Z., Li, J., Wang, S., Liu, Y., Xin, H. (2018, February). Concrete filled tubular arch modified-VFT bridge and its LLSI analysis. In 2017 3rd International Forum on Energy, Environment Science and Materials (IFEESM 2017) (pp. 1379-1382). Atlantis Press. https://doi.org/10.2991/ifeesm-17.2018.250

Yan, Q., Zhang, Z., Yan, J., Laflamme, S. (2021). Analysis of flexural capacity of a novel straight-side U-shaped steel-encased concrete composite beam. Engineering Structures, 242, 112447. https://doi.org/10.1016/j.engstruct.2021.112447

Yang, F., Liu, Y., Xin, H. (2018). Positive bending capacity prediction of composite girders based on elastoplastic cross-sectional analysis. Engineering Structures 167: 327-339.

Zanon, R., Seidl, G., Rademacher, D. (2021). New ideas for steel-concrete composite bridges overpassing highways–VFT-RS technology. ce/papers, 4(2-4): 269-278.

Zhang, G., Kodur, V., Song, C., He, S., Huang, Q. (2020). A numerical model for evaluating fire performance of composite box bridge girders. Journal of Constructional Steel Research 165: 105823. https://doi.org/10.1016/j.jcsr.2019.105823

Zhou, X., Zhao, Y., Liu, J., Chen, Y. F., Yang, Y. (2019). Bending experiment on a novel configuration of cold-formed U-shaped steel-concrete composite beams. Engineering Structures 180: 124-133.